minerals

MDPI

Article

Geochronological Constraints on the Origin of the Paleoproterozoic Qianlishan Gneiss Domes in the Khondalite Belt of the North China Craton and Their Tectonic implications

Hengzhong Qiao [1,2,*], Peipei Deng [2] and Jiawei Li [2]

[1] Department of Geology, Northwest University, Xi'an 710069, China
[2] College of Tourism and Geographical Science, Leshan Normal University, Leshan 614000, China
* Correspondence: qiaohzh@lsnu.edu.cn

Abstract: The Paleoproterozoic gneiss domes are important structures of the Khondalite Belt in the northwestern North China Craton. However, less attention has been paid to their formation and evolution, and it thus hampers a better understanding of the deformation history of the Khondalite Belt. In this paper, we conducted structural and geochronological studies on the Qianlishan gneiss domes of the Khondalite Belt. The field observations and zircon U–Pb dating results show that the Qianlishan gneiss domes consist of 2.06–2.01 Ga granitoid plutons in the core, rimmed by granulite facies metasedimentary rocks (khondalites) of the Qianlishan Group. Both of them were subjected to two major phases of deformation (D1–D2) in the late Paleoproterozoic. Of these, D1 deformation mainly generated overturned to recumbent isoclinal folds F1 and penetrative transposed foliations/gneissosities S1 at ~1.95 Ga. Subsequently, D2 deformation produced the NW(W)–SE(E)-trending doubly plunging upright folds F2 at 1.93–1.90 Ga, and they have strongly re-oriented S1 gneissosities, giving rise to the Qianlishan gneiss domes. Combined with previous studies, we argue that the Qianlishan gneiss domes were the products of the Paleoproterozoic collisional orogenesis between the Yinshan and Ordos Blocks. Additionally, the development of doubly plunging antiforms is considered an important dome-forming mechanism in the Khondalite Belt.

Keywords: gneiss dome; zircon U–Pb dating; Paleoproterozoic; Qianlishan Complex; Khondalite Belt; North China Craton

Citation: Qiao, H.; Deng, P.; Li, J. Geochronological Constraints on the Origin of the Paleoproterozoic Qianlishan Gneiss Domes in the Khondalite Belt of the North China Craton and Their Tectonic implications. *Minerals* **2023**, *13*, 1361. https://doi.org/10.3390/min13111361

Academic Editor: Jaroslav Dostal

Received: 5 September 2023
Revised: 20 October 2023
Accepted: 22 October 2023
Published: 25 October 2023

1. Introduction

Gneiss domes are important features of many orogenic belts around the world, characterized by domal structures that typically comprise granitoid plutons or high-grade metamorphic rocks in the core, with outward-dipping gneissic foliations [1–5]. Most gneiss domes tend to display elliptical or elongated shapes in map view, and their long axes are commonly parallel to the strike of orogens [3,6]. Although gneiss domes show some similarities in geometry, petrology, and structure, a variety of dome-forming mechanisms have been proposed, mainly including diapirism driven by density inversion, buckling under horizontal contraction, extension-controlled exhumation, superposition of multiple deformations, duplex-induced folding, or some combination of these processes [7–11]. The potential link between doming and fundamental orogenic processes (e.g., crustal melting, flow, and exhumation) highlights the significance of the anatomy of gneiss domes in comprehensively understanding the geodynamics of orogens [3]. Of these, a prerequisite for unraveling the origin of gneiss domes is to determine temporal and spatial relationships between major structures, magmatic intrusions, and gneiss domes [2,4].

The Qianlishan Complex is a high-grade gneiss terrain located in the western segment of the Khondalite Belt that has been widely accepted as a Paleoproterozoic collisional orogen in the northwestern North China Craton (Figure 1) [12–17]. Of particular interest is the occurrence of a series of nearly orogen-parallel elongated gneiss domes in this region,

together called the Qianlishan gneiss domes (Figure 2) [18–20]. These gneiss domes are dominated by granitoid plutons in the core and medium- to high-pressure granulite facies metasedimentary rocks of the Qianlishan Group in the rim, respectively (Figure 2) [18]. Notably, previous geochronological, metamorphic, and structural studies have primarily focused on the Qianlishan Group [14–21], but comparatively less attention was paid to the plutonic cores and domal structures in the Qianlishan Complex. Consequently, the origin of the Qianlishan gneiss domes still remains enigmatic, which hinders a comprehensive understanding of the deformation history of the Khondalite Belt. To resolve these key issues, we carried out detailed structural investigations on the Qianlishan gneiss domes and conducted LA-ICP-MS zircon U–Pb dating on granitoid plutons and leucocratic dykes that were variably involved in these domal structures. Integrated with previous studies, field observations and geochronological data in this paper will provide important insights into the development of the Qianlishan gneiss domes and further help to understand the tectonic evolution of the Khondalite Belt.

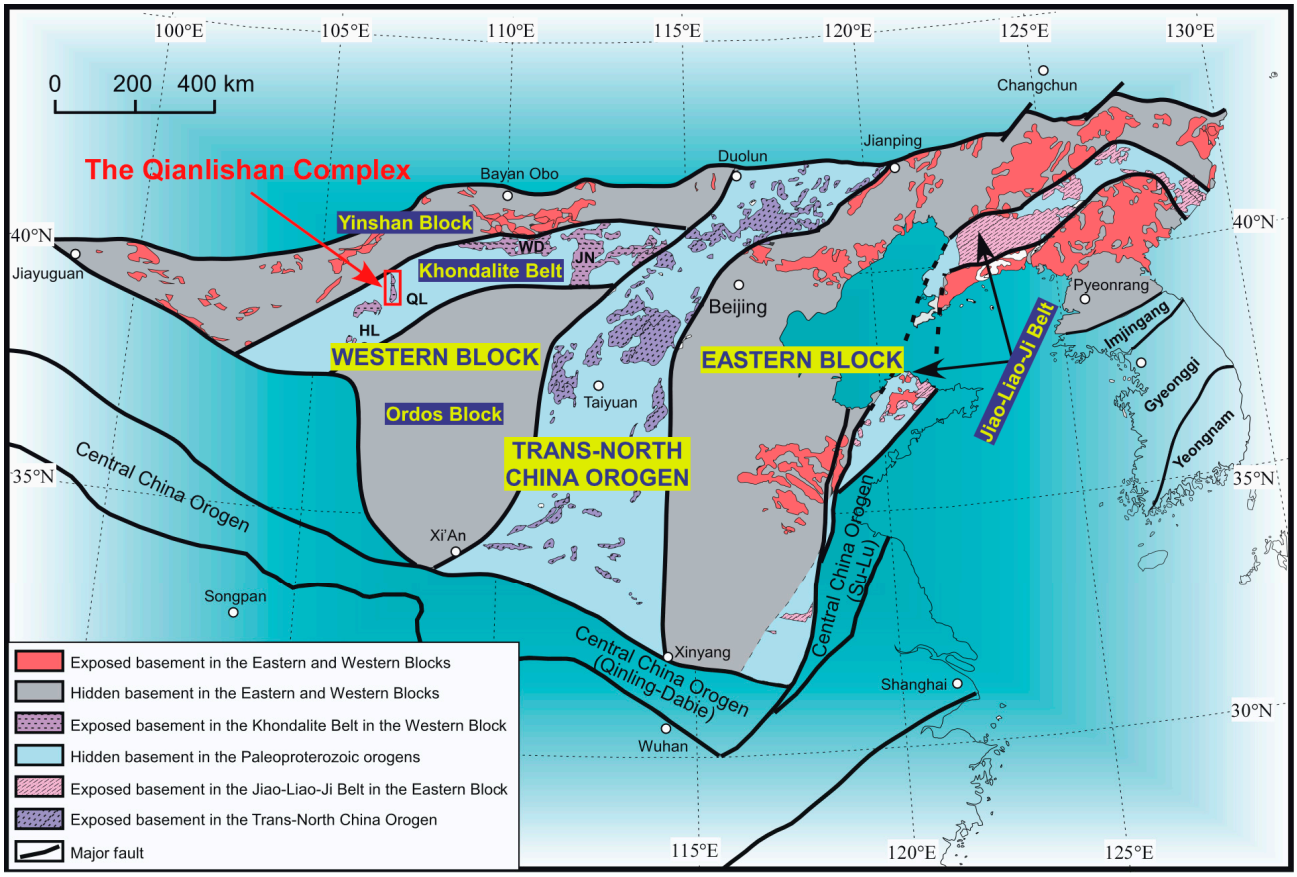

Figure 1. Tectonic subdivision of the North China Craton (modified after [12]). Abbreviations for the exposed high-grade metamorphic complexes in the Khondalite Belt: HL, Helanshan Complex; QL, Qianlishan Complex; WD, Wulashan and Daqingshan complexes; JN, Jining Complex.

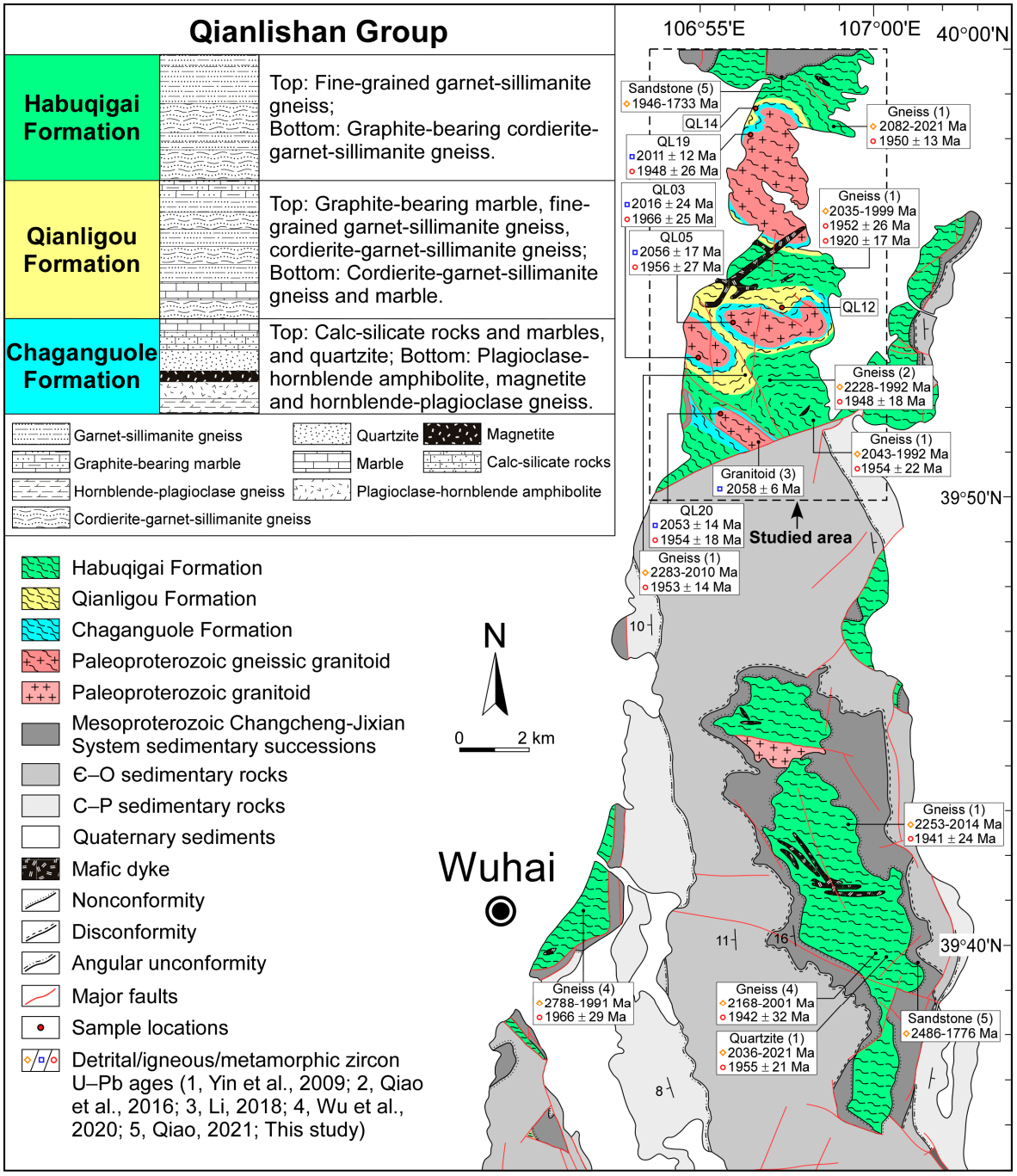

Figure 2. Simplified geological map of the Qianlishan Complex (modified after [14,18–20]).

2. Geological Setting

The North China Craton is amongst the oldest cratons in the world, and it has been regarded to result from the assembly of several Archean to Paleoproterozoic micro-blocks along linear structural belts [12,13,22–25]. The Khondalite Belt is a nearly ~1000 km, E-W-trending collisional orogen, where the northern Yinshan Block has been considered to amalgamate with the southern Ordos Block to form the Western Block at ~1.95 Ga [12–14,26–28]. From west to east, the Khondalite Belt well exposes the Helanshan, Qianlishan, Wulashan, Daqingshan, and Jining Complexes (Figure 1) [12]. These complexes are dominated by upper amphibolite to granulite facies metasedimentary rocks (i.e., the khondalites), mainly including felsic paragneisses, graphite-bearing pelitic gneisses, garnet-bearing quartzites, marbles, and calc-silicate rocks [18,29–31]. The khondalites are spa-

tially juxtaposed with dioritic–granitic gneisses, S-type granites, minor charnockites, and mafic granulites [18,31]. Traditionally, the protoliths of the khondalites were inferred to form on a stable continental margin [12,18,32,33], but recently an active continental margin has also been proposed [34–38]. Extensive geochronological data revealed that the protoliths of khondalites were primarily sourced from a 2.2–2.0 Ga provenance, subsequently deposited at 2.0–1.95 Ga, and experienced regional high-grade metamorphism at 1.95–1.85 Ga [14–17,26,27,39–53]. Ultrahigh temperature (UHT) metamorphism was also regarded to coevally appear throughout the Khondalite Belt [28,54–61]. Moreover, syn- and post-collisional S-type granites that resulted from partial melting of the khondalites are mostly dated at ~1.95 Ga, 1.93–1.90 Ga, and 1.88–1.84 Ga [14,35,36,46,52,62–65].

The Qianlishan Complex is one of the most representative litho-tectonic units in the Khondalite Belt and unconformably overlain by (sub-)horizontal to gently-dipping unmetamorphosed Mesoproterozoic sedimentary sequences of the Changcheng–Jixian System (Figure 2) [18,66]. This complex mainly consists of the Paleoproterozoic granitoid plutons and the khondalites that are termed the Qianlishan Group [18]. The Qianlishan Group is subdivided into the Chaganguole, Qianligou, and Habuqigai formations. Their typical rock assemblages and distributions are shown in Figure 2. Metamorphic studies demonstrate that pelitic and felsic granulites recorded similar clockwise P-T paths, of which pelitic granulites were characterized by peak high-pressure metamorphism and post-peak near-isothermal decompression processes, with their P-T conditions constrained at 11–15 kbar/800–850 °C and 5.7–6.2 kbar/800–815 °C [15,17], respectively. Available U–Pb data show that detrital zircons from the Qianlishan Group mainly gave apparent $^{207}Pb/^{206}Pb$ ages (discordance degree < 10%) ranging from 2788 Ma to 1991 Ma [14,16,17]. Metamorphic zircons dominantly yielded a major age group at ~1.95 Ga that was interpreted as the timing of granulite facies metamorphism in the Qianlishan Complex [14,16,17]. Minor ~1.92 Ga metamorphic zircons were also reported, which were related to post-peak decompression [14]. Meanwhile, a crystallization mean age of 2058 ± 6 Ma was obtained from a granitoid pluton in the Qianligou quarry [37,67], but other plutons in the studied area lacked age constraints. In addition, previous structural investigations revealed that the Qianlishan Group underwent two major stages of deformation (D1–D2) in the Paleoproterozoic [19,20]. D1 deformation was regarded to has occurred at 1976–1936 Ma, characterized by small-scale overturned to recumbent isoclinal folds F1, transposition foliations S1 with NNE-SSW mineral lineations L1 [19,20]. D2 deformation mainly produced NW(W)–SE(E)-trending doubly plunging upright folds F2, and it is inferred to broadly take place at 1936–1854 Ma [19,20].

3. Samples and Methods

Field-based structural investigations were carried out to document the geometry of the Qianlishan gneiss domes. Particularly, domal structures (e.g., foliations, fold hinges) have been analyzed and measured in four representative domains of the studied area (Figure 3a). In order to put age constraints on the development of these gneiss domes, we conducted zircon U–Pb dating on six critical rock samples. Of these, four samples were from gneissic granitoid plutons (Samples QL03, 05, 19, and 20), and the other two samples were from deformation-related leucocratic dykes (Samples QL14 and 12). Zircon U–Pb analyses were performed by LA-ICP-MS at the Guangzhou Tuoyan Analytical Technology Co., Ltd., Guangzhou, China. Detailed analytical procedures were similar to those described in [68]. Laser sampling was conducted using an NWR 193 nm ArF excimer laser ablation system, and an iCAP RQ quadrupole ICP-MS instrument was used to acquire ion-signal intensities. The frequency and spot size of the laser were set to 5 Hz and 30 μm. Zircon 91500 [69] and glass NIST610 [70] were used as external standards for U–Pb dating and trace element calibration, respectively. Zircon standard Plešovice [71] was used as an unknown sample to monitor the working state of the instrument. Each analysis incorporated a background acquisition of approximately 30 s, followed by 40 s of data acquisition from the sample. An Excel-based software, ICPMSDataCal [72], was used to perform offline

selection and integration of background and analyzed signals, time-drift correction, and quantitative calibration for U–Pb dating and trace element analysis. Concordia diagrams and age calculations were made using Isoplot/Ex_ver4.15 [73]. Individual analyses have been presented at 1σ level, and uncertainties on the weighted mean age, lower and upper intercept age were quoted at the 95% confidence level (2σ). Zircon U–Pb data in this study were provided as Supplementary Materials (Table S1).

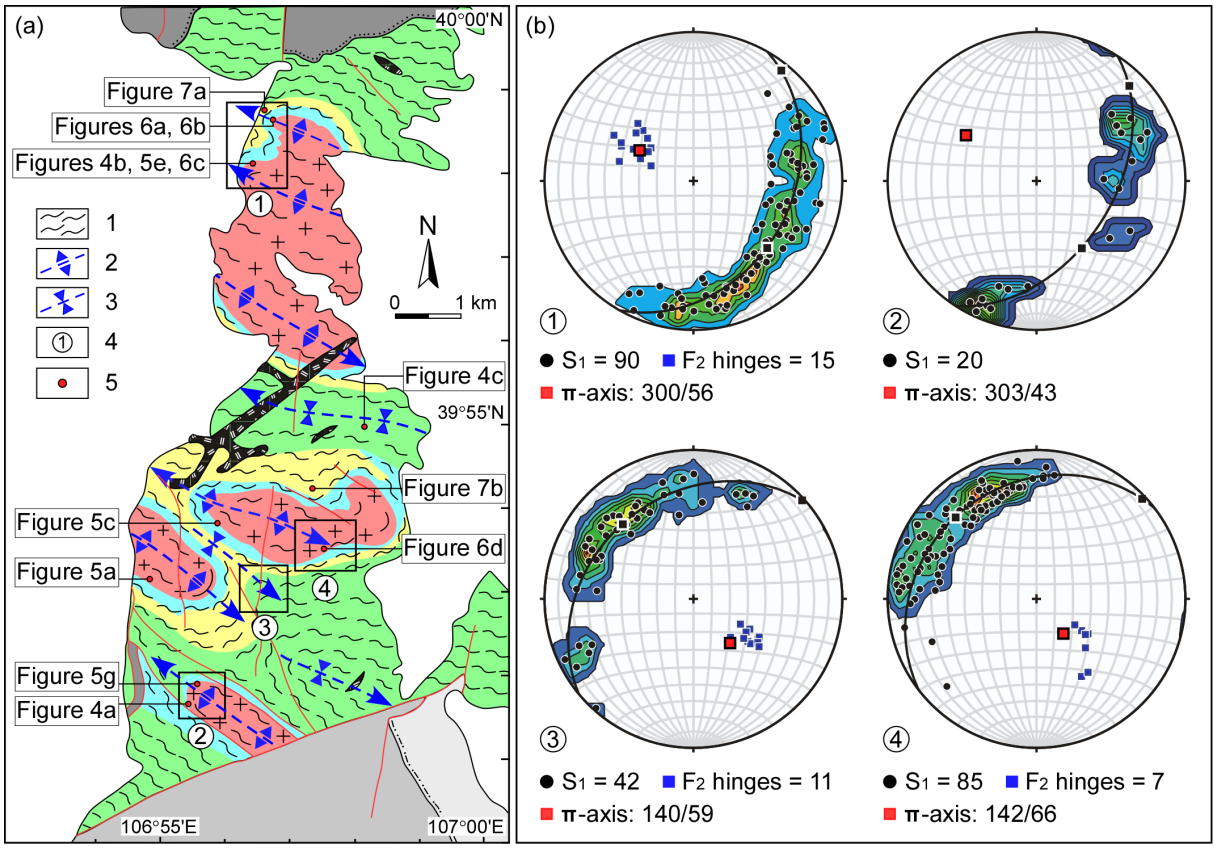

Figure 3. Simplified structural map and stereonet diagrams of the Qianlishan gneiss domes. (**a**) Litho-tectonic map mainly showing structural features of the regional-scale NW(W)–SE(E)-trending doubly plunging upright folds F2 and the penetrative gneissosities S1 (modified after [14,19,20]). 1, S1 gneissosity; 2, F2 antiform; 3, F2 synform; 4, domain for stereonet projection; 5, photo location. (**b**) Stereonet diagrams (lower hemisphere equal-area projections) exhibiting the orientations of S1 gneissosities and F2 fold hinges in four representative areas (domains 1–4 in Figure 3a).

4. Results

4.1. Field Structural Observations

The Qianlishan gneiss domes are exposed in the northern part of the Qianlishan Complex, locally covered by Quaternary sediments. In map view, they are unevenly spaced and roughly display NW(W)–SE(E)-trending elliptical shapes with outward-dipping gneissic foliations (Figure 3a). These domes consist of granitoid plutons in the core, rimmed by high-grade metasedimentary rocks from the Chaganguole, Qianligou, and Habuqigai formations of the Qianlishan Group (Figures 2 and 3), but their metamorphic grades did not significantly vary. There is no large-scale ductile shear zone observed along the contacts between the core and rim of these domes. Remarkably, the penetrative gneissosity in the plutonic cores and the supracrustal rocks are consistent, showing parallelism with the core/rim contacts (Figures 3a and 4a). Similar to the structural features of the Qianlishan Group [19,20], the granitoid plutons in the core were also subjected to D1–D2 deformation (Figures 4–7). In the field, overturned to recumbent isoclinal folds F1 are infrequent

and difficult to discern in the plutons (Figure 4b), though they commonly appear in the Qianlishan Group (Figure 4c). Whereas these granitoid plutons have obviously developed penetrative gneissosities S1 that are mainly defined by the strong alignment of quartz + plagioclase ± K-feldspar ± biotite ± hornblende (Figure 5).

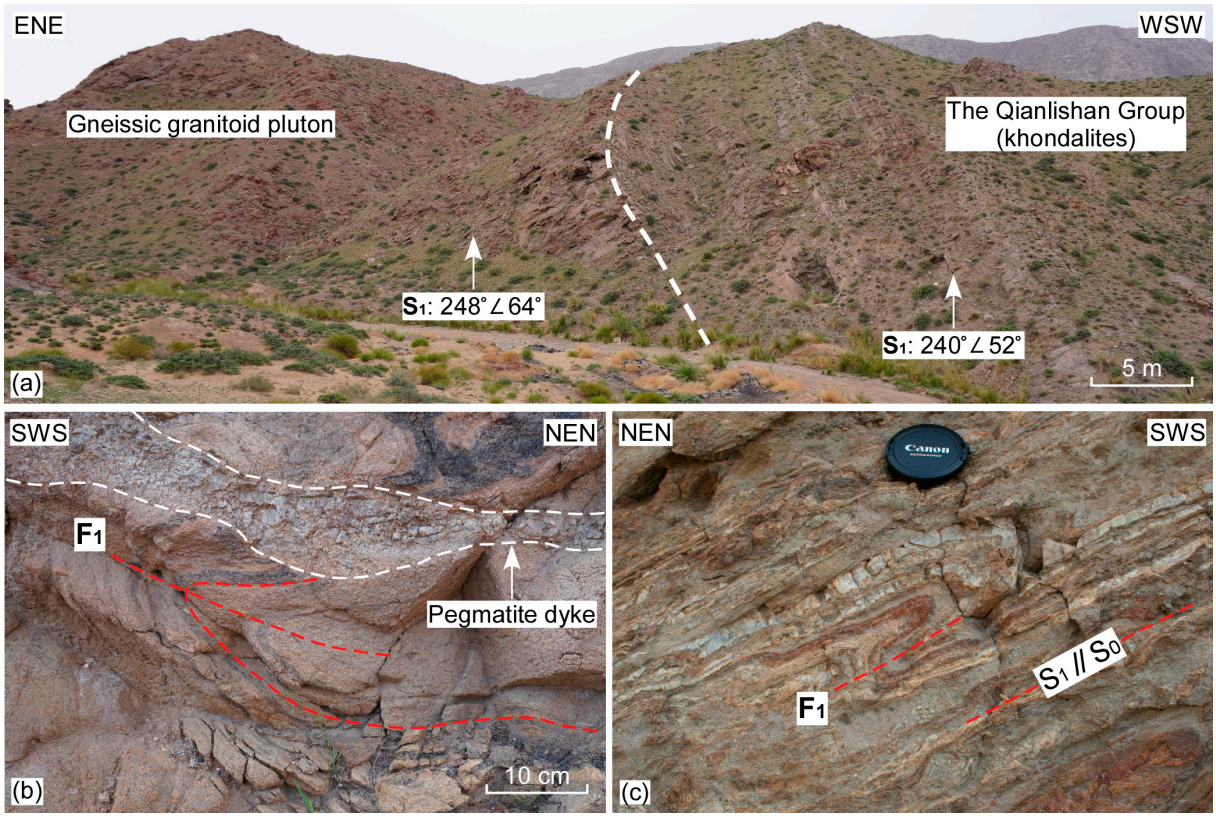

Figure 4. Typical photographs of D1 structures in the Qianlishan gneiss domes. (**a**) The contact between the granitoid pluton in the core and the Qianlishan Group (khondalites) in the rim of the Qianlishan gneiss domes. (**b**) Recumbent tight to isoclinal folds F1 in the granitoid pluton. (**c**) SSW-vergent overturned isoclinal folds F1 that have intensively transposed sedimentary bedding S0 to newly-developed S1 foliations in marbles and calc–silicate rocks.

D2 deformation is dominantly represented by doubly plunging upright open folds F2. The F2 structures commonly occurred as a series of micro- to macroscopic antiforms and synforms with NW(W)–SE(E)-striking sub-vertical fold axial surfaces (Figures 6 and 7). These F2 folds have strongly reworked the previous D1 structures in the metasedimentary rocks and the plutonic cores of the Qianlishan gneiss domes (Figures 6 and 7). Regionally, the F2 folds show doubly plunging geometry, and their fold hinges plunge to either NW(W) or SE(E) (Figure 3). In this study, the attitudes of S1 gneissosities from four representative F2 fold hinge zones (domains 1–4 in Figure 3a) were plotted on the stereonet. In domains 1 and 2, the poles to S1 gneissosities mostly appear along great circle girdles (Figure 3b), the π-axes of which are located at 300°/56° and 303°/43° (azimuth/plunge), respectively. Whereas the orientations of those π-axes in domains 3 and 4 are plotted at 140°/59° and 142°/66° (Figure 3b). These results are in good agreement with the measurements of F2 fold hinges in the field (Figures 3b, 6 and 7). This also confirms the overprinting relationships between the NW(W)–SE(E)-trending doubly plunging F2 folds and the penetrative gneissosities S1.

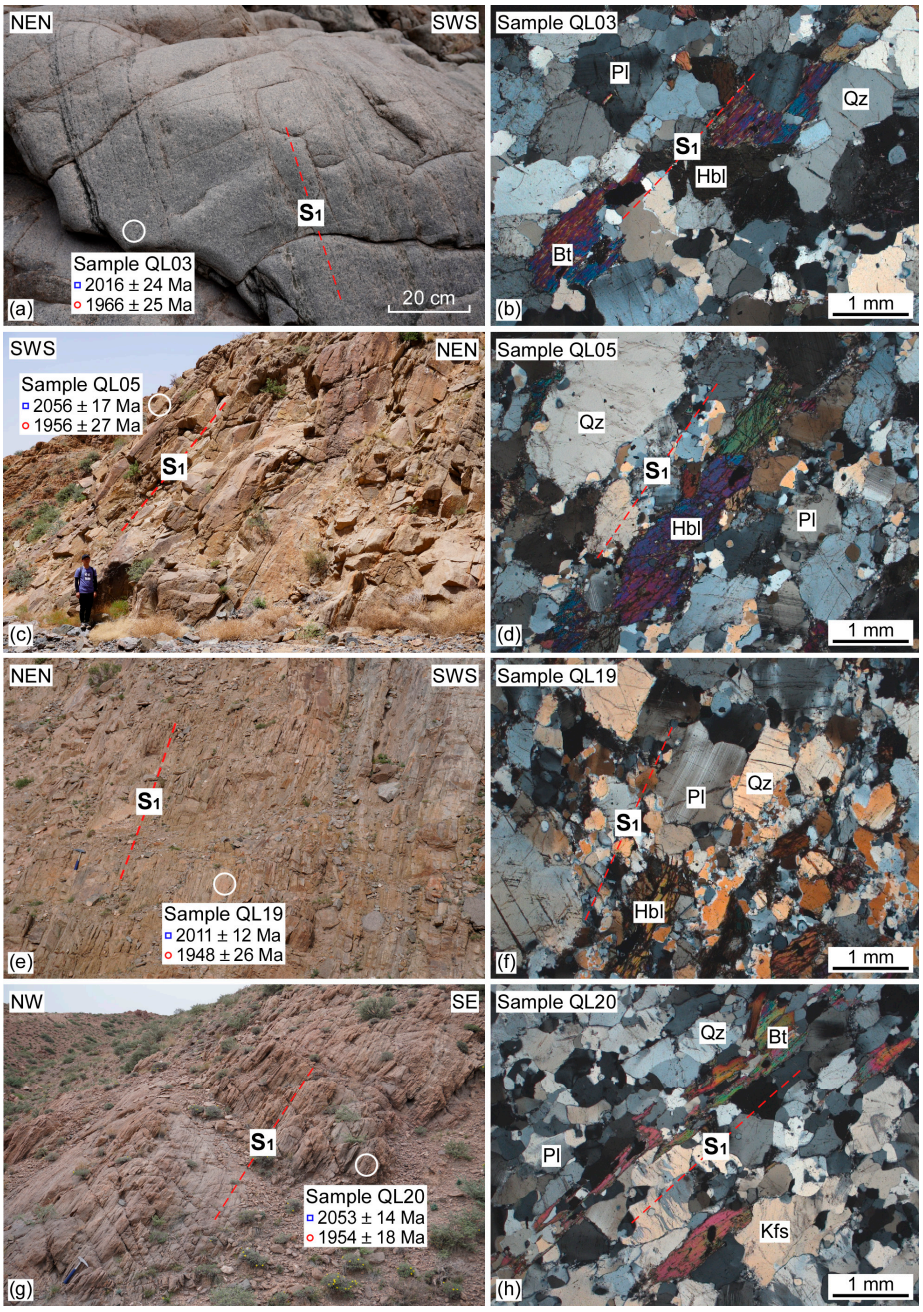

Figure 5. Representative photos of the S1-foliated granitoid plutons in the core of the Qianlishan gneiss domes. (**a**,**b**) The granitoid pluton (Sample QL03) underwent D1 deformation and developed ubiquitous gneissosities S1 that are mainly defined by well-oriented aggregates of quartz, plagioclase, and hornblende (cross-polarized light). (**c**,**d**) The gneissic granitoid plutons (Sample QL05) with pervasive S1 foliations, featured by the preferred alignment of quartz, plagioclase, and hornblende (cross-polarized light). (**e**,**f**) The pluton (Sample QL19) has apparently been foliated during D1 deformation, mainly composed of aligned aggregates of quartz, plagioclase, and hornblende (cross-polarized light). (**g**,**h**) The penetratively S1-foliated granitoid pluton (Sample QL20) is characterized by the preferential orientation of quartz, K-feldspar, plagioclase, and biotite (cross-polarized light). Blue squares and red circles indicate U–Pb ages of magmatic and metamorphic zircons, respectively. Qz, quartz; Pl, plagioclase; Hbl, hornblende; Kfs, K-feldspar; Bt, biotite.

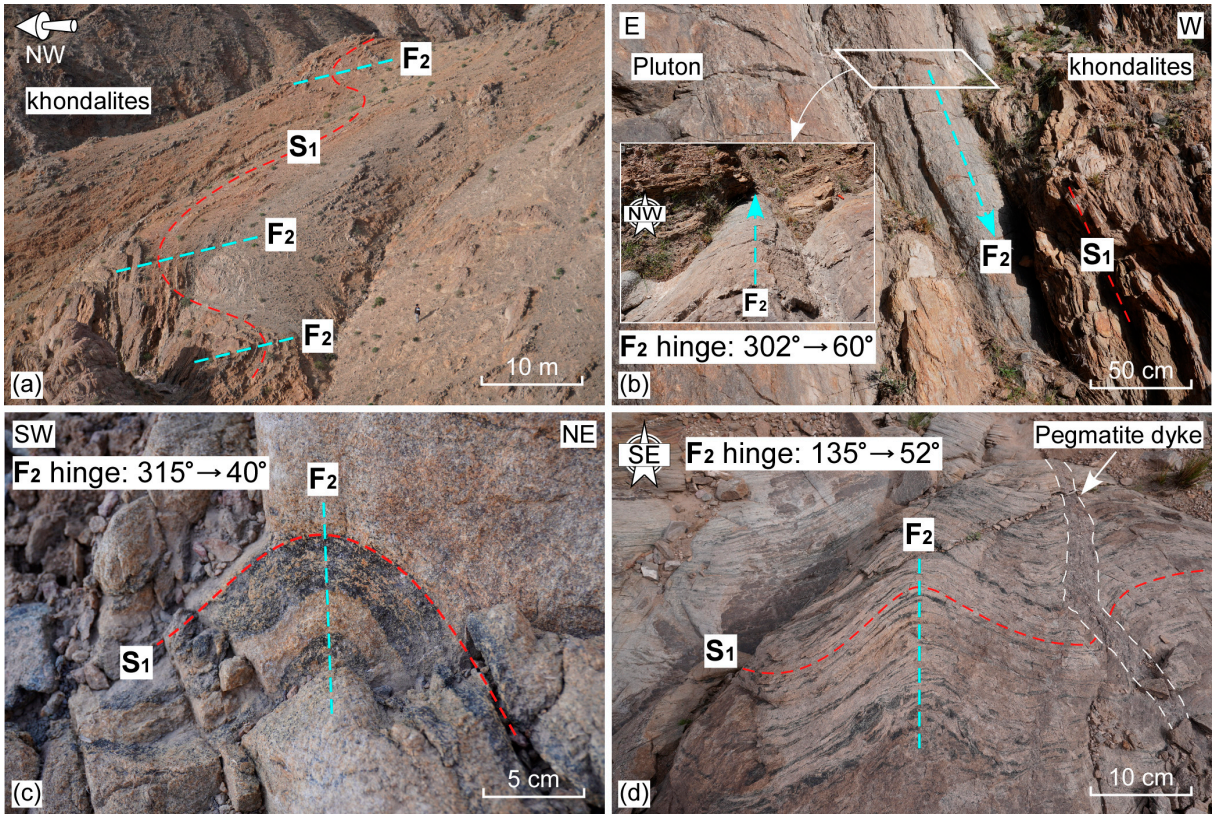

Figure 6. Typical photos of NW(W)–SE(E)-trending doubly plunging folds F2 in the Qianlishan gneiss domes. (**a**) Mesoscopic upright folds F2 that mostly plunge to NW(W) in the Qianlishan Group. (**b**) Open upright folds F2 with moderately NW(W)-plunging fold hinges formed along the core/rim contact of the Qianlishan gneiss domes. (**c**,**d**) Moderately NW- and SE-plunging open folds F2 with vertical fold axial surfaces have reworked the S1 gneissosities in the granitoid pluton.

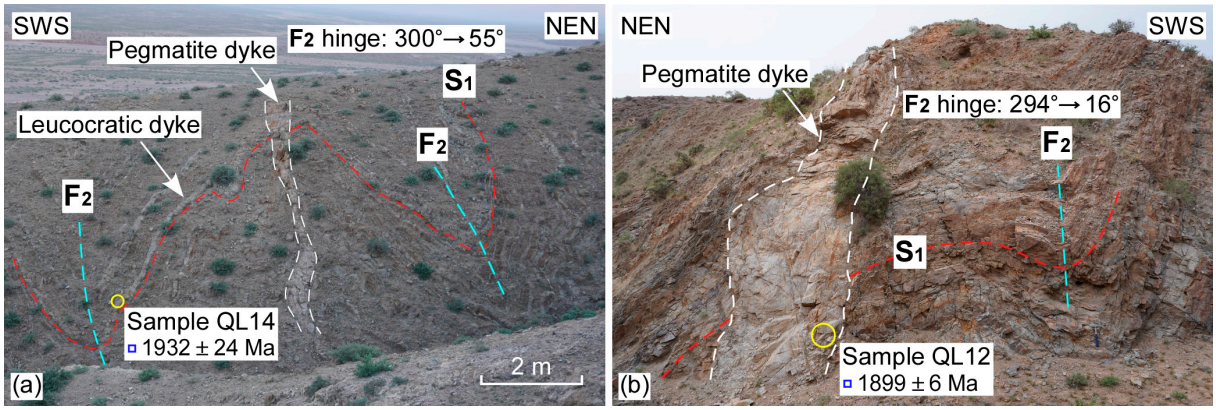

Figure 7. Field photos of two representative leucocratic dykes that displayed different structural features in the Qianlishan gneiss domes. (**a**) A fine-grained leucocratic dyke (Sample QL14) along the pervasive S1 foliations was deflected by moderately NW-plunging open upright folds F2, suggesting that it most likely formed earlier than D2 deformation. (**b**) An undeformed coarse-grained pegmatite dyke (Sample QL12) obliquely truncated the limbs of gently NWW-plunging open upright folds F2, probably indicative of its post-D2 intrusion.

4.2. Zircon U–Pb Geochronology

4.2.1. S1-Foliated Granitoid Plutons

Four representative granitoid gneisses (Samples QL03, 05, 19, and 20) were collected from four plutons in the core of the Qianlishan gneiss domes (39°53.0′ N/106°55.3′ E, 39°54.0′ N/106°55.9′ E, 39°58.3′ N/106°56.8′ E, and 39°51.9′ N/106°55.7′ E; Figure 2), respectively. Zircons separated from these samples are mostly euhedral to subhedral and vary from 100–250 μm in grain size. Cathodoluminescence (CL) images illustrate that they are characterized by typical core–rim textures (Figure 8a–d), of which the zircon cores are commonly bright and oscillatory-zoned, interpreted to be of magmatic origin. These zircon cores are generally surrounded by relatively dark and structureless overgrowth rims (Figure 8a–d), typical of metamorphic origin.

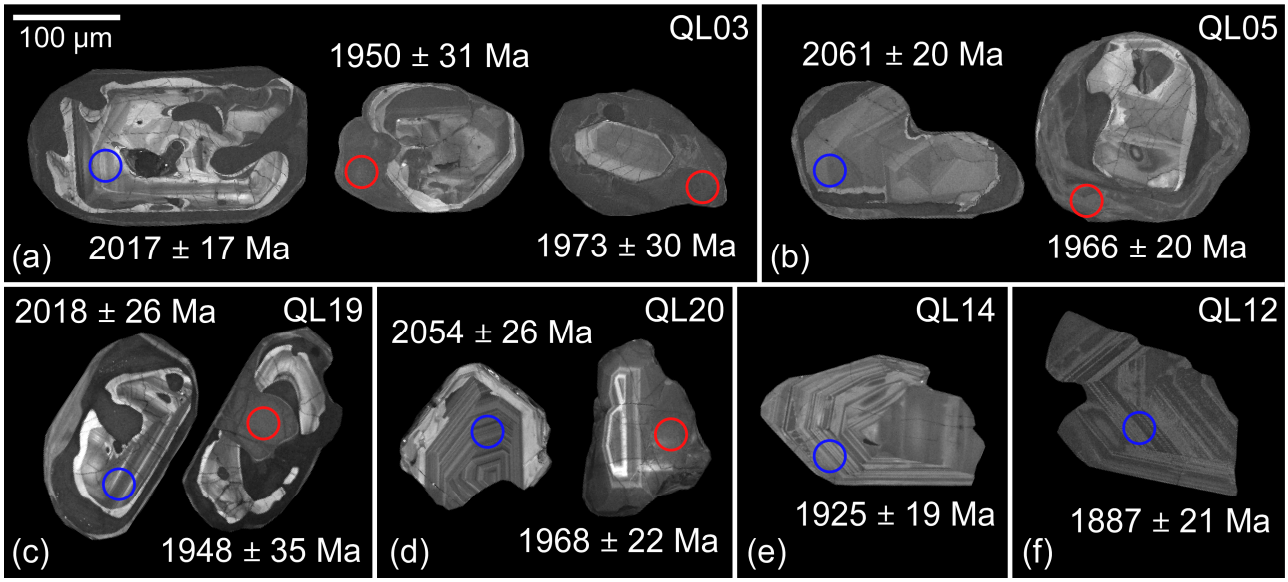

Figure 8. Representative cathodoluminescence (CL) zircon images with their LA-ICP-MS U–Pb ages of dating samples from the Qianlishan gneiss domes. (**a**–**d**) The S1-foliated granitoid plutons (Samples QL03, 05, 19, and 20). (**e**) The pre-D2 F2-folded leucocratic dyke (Sample QL14). (**f**) The post-D2 F2-cutting undeformed pegmatite dyke (Sample QL12). Blue circle, magmatic zircon; red circle, metamorphic overgrowth rim.

(1) Sample QL03

A total of 22 zircons have been analyzed in this sample, and the dating results are presented in Figure 9a and Table S1. Of these, five spots (discordance degree ≤ 5%) were made on the zircon cores of igneous origin (Figure 8a), with high Th/U values of 0.51–1.8. They yielded a weighted mean $^{207}Pb/^{206}Pb$ age of 2016 ± 24 Ma (n = 5, MSWD = 3.4; Figure 9a). The remaining 17 spots on metamorphic overgrowth rims (Figure 8a) have lower Th/U values of 0.02–0.25 (Table S1), and they were variably discordant, probably due to the loss of Pb. On the concordia diagram (Figure 9a), these data define a discordia line with the lower and upper intercept age of 567 ± 29 Ma and 1966 ± 25 Ma (n = 17, MSWD = 8.0), respectively.

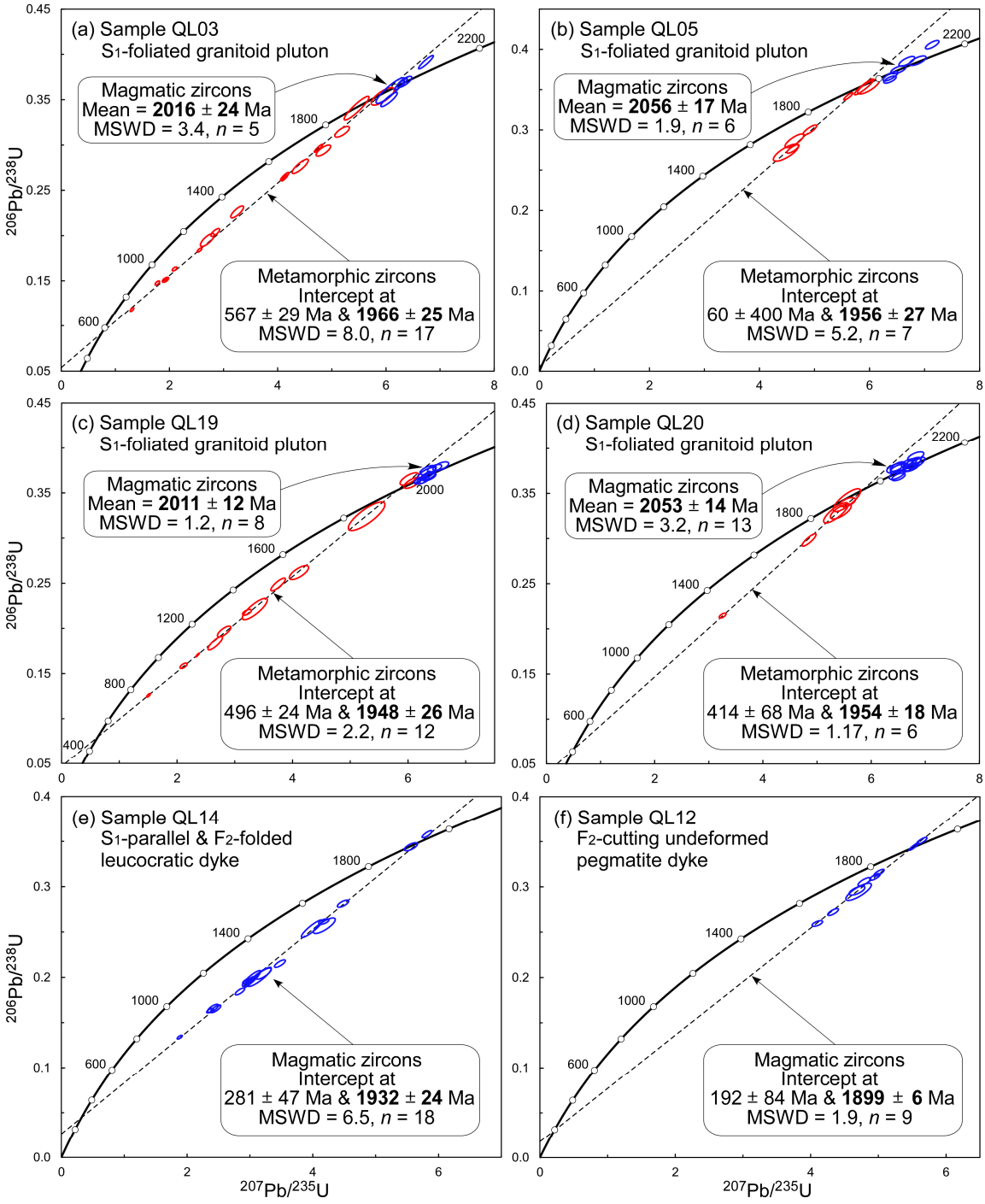

Figure 9. Concordia diagram of LA-ICP-MS zircon U–Pb dating results from the Qianlishan gneiss domes. (**a**–**d**) The S1-foliated granitoid plutons (Samples QL03, 05, 19, and 20). (**e**) The pre-D2 F2-folded leucocratic dyke (Sample QL14). (**f**) The post-D2 F2-cutting undeformed pegmatite dyke (Sample QL12). Blue ellipse, magmatic zircon; red ellipse, metamorphic overgrowth rim. Uncertainties on weighted mean age, lower and upper intercept age were quoted at the 95% confidence level (2σ).

(2) Sample QL05

Six spots (discordance degree ≤ 3.7%; Table S1) were conducted on the magmatic zircon cores in Sample QL05, and they gave a weighted mean $^{207}Pb/^{206}Pb$ age of 2056 ± 17 Ma (n = 6, MSWD = 1.9; Figures 8b and 9b). Meanwhile, seven spots were analyzed on metamorphic overgrowth rims, and they yielded the lower and upper intercept age of 60 ± 400 Ma and 1956 ± 27 Ma (n = 7, MSWD = 5.2; Figures 8b and 9b), respectively.

(3) Sample QL19

A total of 20 zircons were analyzed in this sample, of which eight spots on the igneous zircon cores were concordant (discordance degree ≤ 3.1%; Table S1), yielding a weighted mean $^{207}Pb/^{206}Pb$ age of 2011 ± 12 Ma (n = 8, MSWD = 1.2; Figures 8c and 9c). The remaining 12 spots were undertaken on zircon overgrowth rims of metamorphic origin (Figure 8c) and defined the lower and upper intercept age of 496 ± 24 Ma and 1948 ± 26 Ma (n = 12, MSWD = 2.2; Figure 9c), respectively.

(4) Sample QL20

Thirteen spots (discordance degree ≤ 4.1%; Table S1) were carried out on the magmatic zircon cores in Sample QL20 and gave a weighted mean $^{207}Pb/^{206}Pb$ age of 2053 ± 14 Ma (n = 13, MSWD = 3.2; Figures 8d and 9d). Another six analyses were obtained from metamorphic overgrowth rims and yielded the lower and upper intercept age of 414 ± 68 Ma and 1954 ± 18 Ma (n = 6, MSWD = 1.17; Figures 8d and 9d), respectively.

4.2.2. F2-Folded Leucocratic Dyke

Sample QL14 was collected from a fine-grained leucocratic dyke that intruded the Qianligou Formation in the northern part of the Qianlishan Complex (Figure 2; 39°58.8′ N/106°56.9′ E). In the field, this dyke appeared along the S1 foliations of the host metasedimentary rocks (Figure 7a), which were together deflected by the moderately NWW-plunging upright open folds F2. The dyke mainly exhibited granitic textures and did not develop any D1 deformational fabrics. These features indicate that the dyke most likely formed after D1 deformation but prior to D2 deformation. Zircons from Sample QL14 are euhedral, prismatic, and 150–200 μm in grain size. CL images reveal that they are generally single grains with bright, patchy, or oscillatory zoning (Figure 8e). Meanwhile, most of these zircons have high Th/U values of 0.5–0.9 (Table S1), indicative of magmatic origin [74]. A total of 18 spots were conducted on 18 igneous zircons in this sample. On the concordia diagram (Figure 9e), these data were plotted as a discordia line with the lower and upper intercept age of 281 ± 47 Ma and 1932 ± 24 Ma (n = 18, MSWD = 6.5).

4.2.3. F2-Cutting Undeformed Pegmatite Dyke

Sample QL12 was collected from a coarse-grained pegmatite dyke without deformational fabrics (Figure 2; 39°54.2′ N, 106°57.6′ E). This dyke obliquely cut the limb of a gently NWW-plunging upright open fold F2 (Figure 6b), suggesting that its emplacement postdated D2 deformation. Zircons separated from this sample are 100–200 μm, euhedral to subhedral single grains. In CL images, they are commonly patchy and oscillatory-zoned (Figure 8f). Combined with their Th/U values of 0.33–0.76 (Table S1), these zircons are considered to be of igneous origin [74]. A total of nine zircons were analyzed in the sample, which defined the lower and upper intercept age of 192 ± 84 Ma and 1899 ± 6 Ma (n = 9, MSWD = 1.9; Figure 9f), respectively.

5. Discussions

5.1. Significance of Zircon U–Pb Ages

A critical aspect of understanding the development of gneiss domes is temporal relations among magmatism, deformation, and metamorphism involved in the dome-forming processes [3,4,9]. The granitoid plutons in the core of the Qianlishan gneiss domes have long been inferred to have formed in the Paleoproterozoic [18], but their crystallization

ages were poorly understood. In this study, magmatic zircons from four gneissic granitoid plutons (Samples QL03, 05, 19, and 20; Figures 2 and 5) yielded weighted mean ages of 2016 ± 24 Ma, 2056 ± 17 Ma, 2011 ± 12 Ma, and 2053 ± 14 Ma, respectively (Figures 8a–d, 9a–d and 10). Similarly, previous dating results have revealed a crystallization age of 2058 ± 6 Ma from the same pluton with Sample QL20 [37,67]. These ages suggested that the granitoid plutons were broadly emplaced at 2.06–2.01 Ga. Noticeably, the compilation of available data demonstrates that detrital zircons from the metasedimentary rocks of the Qianlishan Group predominantly gave ages of 2.1–2.0 Ga (discordance degree < 10%) [14,16,17], with a prominent single peak at ~2.02 Ga. This supports that the 2.06–2.01 Ga granitoid plutons have probably provided important clastic sediments for the protoliths of the Qianlishan Group [14,16]. Subsequently, the 2.06–2.01 Ga granitoid plutons have been highly S1-foliated during D1 deformation (Figure 5). Metamorphic zircon overgrowth rims from the plutons (Samples QL03, 05, 19, and 20) yielded upper intercept ages of 1966 ± 25 Ma, 1956 ± 27 Ma, 1948 ± 26 Ma, and 1954 ± 18 Ma (Figures 8a–d, 9a–d and 10), which coincide with those ~1.95 Ga metamorphic ages of pelitic/felsic granulites from the Qianlishan Group [14,16,17], interpreted as the timing of syn-D1 regional metamorphic event. Taken together, we consider that the plutonic cores and khondalites of the Qianlishan gneiss domes underwent regional high-grade metamorphism and coevally developed penetrative S1 gneissosities at ~1.95 Ga (Figure 10). This interpretation is also supported by the assumption that D1 structures in the Qianlishan Group roughly occurred at some time between ~1976 Ma and ~1936 Ma [19,20].

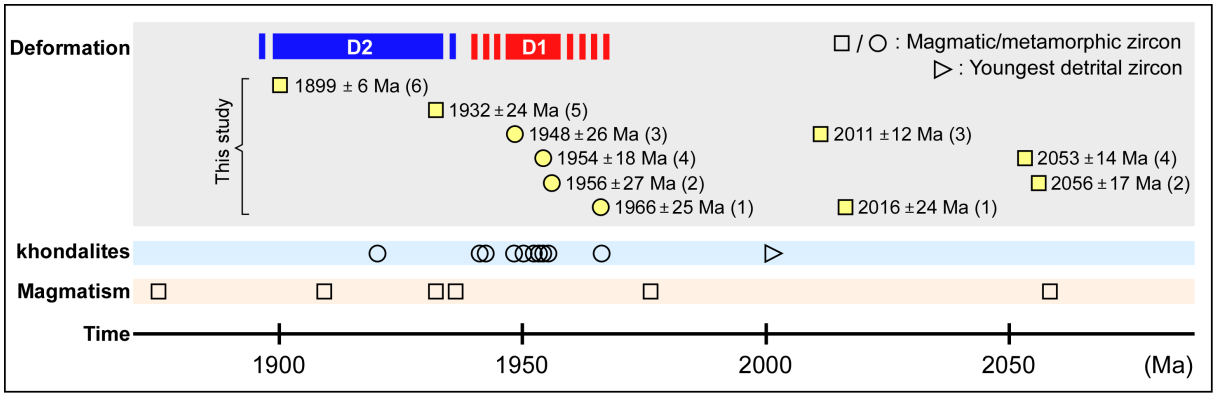

Figure 10. Schematic diagram illustrating temporal relations among major magmatic, deformational, and metamorphic events in the Paleoproterozoic Qianlishan gneiss domes. Dating samples are from this study (1–4, the S1-foliated granitoid plutons, Samples QL03, 05, 19, and 20; 5, the pre-D2 F2-folded leucocratic dyke, Sample QL14; 6, the post-D2 F2-cutting undeformed pegmatite dyke, Sample QL12) and previous studies [14,16,17,19,20,37,67]. See the text for details.

Abundant leucocratic dykes were involved in D2 structures in the Qianlishan gneiss domes, and they provided good opportunities to put age constraints on D2 deformation. Of these, an S1-parallel fine-grained leucocratic dyke (Sample QL14; Figure 7a) has been reworked by the upright open fold F2, interpreted to predate D2 deformation. This pre-D2 dyke yielded an upper intercept age of 1932 ± 24 Ma that was considered as its approximate crystallization age (Figures 8e and 9e), indicating that D2 deformation took place later than ~1.93 Ga. Meanwhile, a similar formation age of 1932 ± 47 Ma was obtained from a syn-D2 dyke that both truncated the S1 gneissosity and appeared along the F2 fold axial surface [19,20]. Later, a series of randomly oriented pegmatite dykes intruded into the Qianlishan Complex, which exhibited clear crosscutting relationships with all the D1 and D2 structures (e.g., Figures 4b, 6d and 7). Based on our observations, an undeformed pegmatite dyke (Sample QL12; Figure 7b) obliquely cut the limb of the F2 fold, indicative of post-D2 intrusion. The dyke gave an upper intercept age of 1899 ± 6 Ma (Figures 8f and 9f), regarded as its crystallization age. This suggests that D2 deformation occurred approxi-

mately earlier than ~1.90 Ga. Consistently, an 1854 ± 68 Ma post-D2 undeformed pegmatite dyke has also been found in this region, implying that D2 deformation was broadly constrained before ~1854 Ma [19,20]. Thus, we further proposed that D2 deformation has most likely happened in the period of 1.93–1.90 Ga (Figure 10). In addition, we note that magmatic zircons from Sample QL14 and 12 yielded lower intercept ages of 281 ± 47 Ma and 192 ± 84 Ma (Figure 9e,f), respectively. Similarly, metamorphic zircons from Samples QL03, 05, 19, and 20 gave lower intercept ages of 567 ± 29 Ma, 60 ± 400 Ma, 496 ± 24 Ma and 414 ± 68 Ma (Figure 9a–d). But these ages are difficult to relate to a known late-stage tectonothermal event in the Khondalite Belt.

5.2. Structural Evolution of the Qianlishan Gneiss Domes

The map-view NW(W)–SE(E)-trending elliptical Qianlishan gneiss domes occupy the northern part of the Qianlishan Complex (Figures 2 and 3a) [18–20], and the cores of these domes are dominated by the 2.06–2.01 Ga granitoid plutons (Figures 3, 5, 9 and 10). Available structural and geochronological data demonstrate that the Qianlishan gneiss domes underwent two major phases of deformation (D1–D2) in the late Paleoproterozoic (Figures 4–7 and 10). Of these, D1 deformation has approximately taken place at ~1.95 Ga, mainly manifested by overturned to recumbent isoclinal folds F1, transposed foliations/gneissosities S1 and NNE-SSW mineral lineations L1 (Figures 4, 5 and 10) [19,20]. The penetrative gneissosities S1 in the core and rim of the Qianlishan gneiss domes are continuous and parallel to the core/rim contacts (Figures 3a and 4a). We interpret these contacts as deformed unconformities between the granitoid plutons and the overlying Qianlishan Group. They can also serve as important markers to trace the Qianlishan gneiss domes in map view (Figures 2 and 3a). Subsequently, D2 deformation generated NW(W)–SE(E)-trending doubly plunging open upright folds F2 at 1.93–1.90 Ga (Figures 6, 7 and 10). D2 deformation apparently lacked the development of ubiquitous foliations, implying that it perhaps happened at a relatively shallower level than D1 deformation. Noticeably, the superposition of D2 on D1 deformation played an important role in shaping the general structural framework of the Qianlishan Complex (Figures 3, 6, 7 and 10). We consider that the doubly plunging open upright antiforms F2 have strongly re-oriented the penetrative gneissosities S1, giving rise to the Qianlishan gneiss domes. This is supported by the fact that a series of regional-scale antiforms and synforms F2 alternatively occurred in the northern Qianlishan Complex (Figures 3, 6 and 7). Meanwhile, the absence of syn-doming large-scale plutonism and radial lineation pattern in this region suggests that the origin of Qianlishan gneiss domes might not be primarily controlled by magmatic diapirism. This interpretation corresponds to the viewpoint that gneiss domes without syn-kinematic plutons can be created by the formation of doubly plunging antiforms [4,9,75].

5.3. Tectonic Implications

As mentioned earlier, high-pressure pelitic/felsic granulites in the Qianlishan Complex recorded clockwise P-T paths with peak conditions of 11–15 kbar/800–850 °C, indicating that they were once buried at lower crustal depths of 45–50 km [15,17]. Previous structural investigations also unraveled that the contractional deformation D1 was associated with peak granulite facies metamorphism at ~1.95 Ga, linked to the continent–continent collision [12–17,19,20]. Later, D2 deformation and post-peak decompression simultaneously occurred, related to tectonic exhumation after crustal thickening [15,17,19,20]. The NW(W)–SE(E)-trending doubly plunging open upright antiforms F2 were responsible for the development of the Qianlishan gneiss domes at 1.93–1.90 Ga. Meanwhile, extensive post-collisional partial melting happened in the Qianlishan Complex, as partly indicated by the presence of ~1.93 Ga and 1.91–1.90 Ga leucocratic dykes (Figure 10) [14,19,20,37,67], which might facilitate dome-forming processes during D2 deformation. Moreover, we regard that D2 doming deformation played an important role in the upward exhumation of high-pressure granulites in the Qianlishan Complex. Taken together, the Qianlishan gneiss

domes are considered to have witnessed the collisional orogenesis between the Yinshan and Ordos Blocks in the late Paleoproterozoic.

Remarkably, dome-like structures that are dominated by 2.3–2.0 Ga gneissic granitoid plutons in the core have also been found in other segments of the Khondalite Belt (e.g., the Daqingshan Complex [76]; the Helanshan Complex [77,78]), but their origin still remains enigmatic. Meanwhile, the D1 and D2 deformational fabrics documented in this study are ubiquitous throughout the Khondalite Belt [18,78–82]. Some authors assumed that D1 structures resulted from sub-horizontal extensional detachment deformation [83–85]. This interpretation is not supported by structural observations in the Qianlishan Complex, and we attribute D1 deformational fabrics to the nearly NNE–SSW collision between the Yinshan and Ordos Blocks [19,20]. Moreover, the superposition of doubly plunging open upright folds F2 on the penetrative gneissosities S1 is common in the Daqingshan Complex [79], similar to the case of the Qianlishan gneiss domes in this study. We consider that the development of doubly plunging antiforms was an important dome-forming mechanism in the Khondalite Belt. Additionally, it is worth noting that the Qianlishan gneiss domes are well-preserved, but domal structures in other complexes were variably reworked by post-D2 (ca. 1.89–1.87 Ga) large-scale NE- to E-striking ductile shear zones in the Khondalite Belt [19,61,86].

6. Concluding Remarks

Based on our new structural and geochronological data, the Qianlishan gneiss domes consist of 2.06–2.01 Ga granitoid plutons in the core, rimmed by high-grade metasedimentary rocks of the Qianlishan Group. They were subjected to regional high-grade metamorphism and D1 deformation at ~1.95 Ga, mainly characterized by overturned to recumbent isoclinal folds F1 and penetrative transposed gneissosities S1. Subsequently, D2 deformation produced the NW(W)–SE(E)-trending doubly plunging upright folds F2 that have strongly re-oriented S1 gneissosities at 1.93–1.90 Ga, responsible for the origin of the Qianlishan gneiss domes. Combined with previous studies, we consider that the Paleoproterozoic Qianlishan gneiss domes have resulted from the collisional orogenesis between the Yinshan and Ordos Blocks. In addition, the development of doubly plunging antiforms is regarded as an important dome-forming mechanism in the Khondalite Belt.

Supplementary Materials: The following supporting information can be downloaded at https://www.mdpi.com/article/10.3390/min13111361/s1, Table S1: LA-ICP-MS zircon U–Pb data for dating samples from the Qianlishan gneiss domes.

Author Contributions: Conceptualization, H.Q.; investigation, H.Q. and J.L.; methodology, H.Q. and P.D.; data curation, H.Q. and P.D.; writing—original draft preparation, H.Q., P.D. and J.L.; writing—review and editing, H.Q.; supervision, H.Q.; funding acquisition, H.Q.; All authors have read and agreed to the published version of the manuscript.

Funding: This research was funded by National Natural Science Foundation of China (Grant No. 42002221), China Postdoctoral Science Foundation (Grant No. 2022M712569), Science & Technology Department of Sichuan Province (Grant No. MZGC20230103) and Leshan Normal University (Grant No. KYCXTD2023-2, RC202009, LZD031).

Data Availability Statement: Not applicable.

Conflicts of Interest: The authors declare no conflict of interest.

References

1. Eskola, P.E. The problem of mantled gneiss domes. *Q. J. Geol. Soc.* **1948**, *104*, 461–476. [CrossRef]
2. Hobbs, B.E.; Means, W.D.; Williams, P.F. *An outline of Structural Geology*; Wiley: New York, NY, USA, 1976; pp. 428–430.
3. Whitney, D.L.; Teyssier, C.; Vanderhaeghe, O. Gneiss domes and crustal flow. In *Gneiss Domes in Orogeny*; Whitney, D.L., Teyssier, C., Siddoway, C.S., Eds.; Geological Society of America: Boulder, CO, USA, 2004; Volume 380, pp. 15–34.
4. Yin, A. Gneiss domes and gneiss dome systems. In *Gneiss Domes in Orogeny*; Whitney, D.L., Teyssier, C., Siddoway, C.S., Eds.; Geological Society of America Special Paper; Geological Society of America: Boulder, CO, USA, 2004; Volume 380, pp. 1–14.

5. Xu, Z.Q.; Li, Y.; Ji, S.C.; Li, G.W.; Pei, X.Z.; Ma, X.X.; Xiang, H.; Wang, R.R. Qinling gneiss domes and implications for tectonic evolution of the Early Paleozoic Orogen in Central China. *J. Asian Earth Sci.* **2020**, *188*, 104052. [CrossRef]
6. Brun, J.P. The cluster-ridge pattern of mantled gneiss domes in eastern Finland: Evidence for large-scale gravitational instability of the Proterozoic crust. *Earth Planet. Sci. Lett.* **1980**, *47*, 441–449. [CrossRef]
7. Yin, A. Mechanisms for the formation of domal and basinal detachment faults: A three-dimensional analysis. *J. Geophys. Res. Solid Earth* **1991**, *96*, 14577–14594. [CrossRef]
8. Fletcher, R.C. Three-dimensional folding and necking of a power-law layer: Are folds cylindrical, and, if so, do we understand why? *Tectonophysics* **1995**, *247*, 65–83. [CrossRef]
9. Bell, T.H.; Ham, A.P.; Hayward, N.; Hickey, K.A. On the development of gneiss domes. *Aust. J. Earth Sci.* **2005**, *52*, 183–204. [CrossRef]
10. Lee, J.; Hacker, B.; Wang, Y. Evolution of North Himalayan gneiss domes: Structural and metamorphic studies in Mabja Dome, southern Tibet. *J. Struct. Geol.* **2004**, *26*, 2297–2316. [CrossRef]
11. Zhang, B.; Chai, Z.; Yin, C.Y.; Huang, W.T.; Wang, Y.; Zhang, J.J.; Wang, X.X.; Cao, K. Intra-continental transpression and gneiss doming in an obliquely convergent regime in SE Asia. *J. Struct. Geol.* **2017**, *97*, 48–70. [CrossRef]
12. Zhao, G.C.; Sun, M.; Wilde, S.A.; Li, S.Z. Late Archean to Paleoproterozoic evolution of the North China Craton: Key issues revisited. *Precambrian Res.* **2005**, *136*, 177–202. [CrossRef]
13. Zhao, G.C.; Cawood, P.A.; Li, S.Z.; Wilde, S.A.; Sun, M.; Zhang, J.; He, Y.H.; Yin, C.Q. Amalgamation of the North China Craton: Key issues and discussion. *Precambrian Res.* **2012**, *222*, 55–76. [CrossRef]
14. Yin, C.Q.; Zhao, G.C.; Sun, M.; Xia, X.P.; Wei, C.J.; Zhou, X.W.; Leung, W.H. LA-ICP-MS U–Pb zircon ages of the Qianlishan Complex: Constrains on the evolution of the Khondalite Belt in the Western Block of the North China Craton. *Precambrian Res.* **2009**, *174*, 78–94. [CrossRef]
15. Yin, C.Q.; Zhao, G.C.; Wei, C.J.; Sun, M.; Guo, J.H.; Zhou, X.W. Metamorphism and partial melting of high-pressure pelitic granulites from the Qianlishan Complex: Constraints on the tectonic evolution of the Khondalite Belt in the North China Craton. *Precambrian Res.* **2014**, *242*, 172–186. [CrossRef]
16. Qiao, H.Z.; Yin, C.Q.; Li, Q.L.; He, X.L.; Qian, J.H.; Li, W.J. Application of the revised Ti-in-zircon thermometer and SIMS zircon U–Pb dating of high-pressure pelitic granulites from the Qianlishan-Helanshan Complex of the Khondalite Belt, North China Craton. *Precambrian Res.* **2016**, *276*, 1–13. [CrossRef]
17. Wu, S.J.; Yin, C.Q.; Davis, D.W.; Zhang, J.; Qian, J.H.; Qiao, H.Z.; Xia, Y.F.; Liu, J.N. Metamorphic evolution of high-pressure felsic and pelitic granulites from the Qianlishan Complex and tectonic implications for the Khondalite Belt, North China Craton. *Geol. Soc. Am. Bull.* **2020**, *132*, 2253–2266. [CrossRef]
18. Lu, L.Z.; Xu, X.C.; Liu, F.L. *Early Precambrian Khondalites in North China*; Changchun Publishing House: Changchun, China, 1996; pp. 1–277. (In Chinese)
19. Qiao, H.Z. Structural and Geochronological Studies of the Qianlishan-Helanshan Complex in North China. Ph.D. Dissertation, Sun Yat-sen University, Guangzhou, China, 2019; pp. 1–163, (In Chinese with English Abstract).
20. Yin, C.Q.; Qiao, H.Z.; Lin, S.F.; Li, C.C. Zhang, J.; Qian, J.H.; Wu, S.J. Deformation history of the Qianlishan complex, Khondalite belt, North China: Structures, ages and tectonic implications. *J. Struct. Geol.* **2020**, *141*, 104176. [CrossRef]
21. He, X.L.; Yin, C.Q.; Long, X.P.; Qian, J.H.; Wang, L.J.; Qiao, H.Z. Archean to Paleoproterozoic continental crust growth in the Western Block of North China: Constraints from zircon Hf isotopic and whole-rock Nd isotopic data. *Precambrian Res.* **2017**, *303*, 105–116. [CrossRef]
22. Zhai, M.G.; Peng, P. Paleoproterozoic events in North China Craton. *Acta Petrol. Sin.* **2007**, *23*, 2665–2682. (In Chinese with English Abstract)
23. Zhai, M.G.; Santosh, M. The early Precambrian odyssey of the North China Craton: A synoptic overview. *Gondwana Res.* **2011**, *20*, 6–25. [CrossRef]
24. Kusky, T.M.; Polat, A.; Windley, B.F.; Burke, K.C.; Dewey, J.F.; Kidd, W.S.F.; Maruyama, S.; Wang, J.P.; Deng, H.; Wang, Z.S.; et al. Insights into the tectonic evolution of the North China Craton through comparative tectonic analysis: A record of outward growth of Precambrian continents. *Earth-Sci. Rev.* **2016**, *162*, 387–432. [CrossRef]
25. Wei, C.; Zhai, M.; Wang, B. Four phases of Orosirian metamorphism in the north North China Craton (NNCC): Insights into the regional tectonic framework and evolution. *Earth-Sci. Rev.* **2023**, *241*, 104449. [CrossRef]
26. Wan, Y.S.; Liu, D.Y.; Xu, Z.Y.; Dong, C.Y.; Wang, Z.J.; Zhou, H.Y.; Yang, Z.S.; Liu, Z.H.; Wu, J.S. Paleoproterozoic crustally derived carbonate-rich magmatic rocks from the Daqinshan area, North China Craton: Geological, petrographical, geochronological and geochemical (Hf, Nd, O and C) evidence. *Am. J. Sci.* **2008**, *308*, 351–378. [CrossRef]
27. Zhou, X.W.; Geng, Y.S. Metamorphic age of the khondalites in the Helanshan region: Constraints on the evolution of the Western block in the North China Craton. *Acta Petrol. Sin.* **2009**, *25*, 1843–1852, (In Chinese with English Abstract).
28. Guo, J.H.; Peng, P.; Chen, Y.; Jiao, S.J.; Windley, B.F. UHT sapphirine granulite metamorphism at 1.93–1.92 Ga caused by gabbronorite intrusions: Implications for tectonic evolution of the northern margin of the North China Craton. *Precambrian Res.* **2012**, *222*, 124–142. [CrossRef]
29. Qian, X.L.; Cui, W.Y.; Wang, S.Q. Evolution of the Inner Mongolia-eastern Hebei Archean Granulite Belt in the North China Craton. In *The Records of Geological Research*; Department of Geology, Beijing University Press: Beijing, China, 1985.

30. Shen, Q.H.; Xu, H.F.; Zhang, Z.Q.; Gao, J.F.; Wu, J.S.; Ji, C.L. *Precambrian Granulites in China*; Geological Publishing House: Beijing, China, 1992.
31. Zhai, M. Khondalite revisited-record of special geological processes on Earth. *Acta Petrol. Sin.* **2022**, *96*, 2967–2997, (In Chinese with English Abstract).
32. Condie, K.C.; Boryta, M.D.; Liu, J.Z. The origin of khondalites: Geochemical evidence from the Archean to Early Proterozoic granulite belt in the North China Craton. *Precambrian Res.* **1992**, *59*, 207–223. [CrossRef]
33. Lu, L.Z.; Jin, S.Q. P-T-t paths and tectonic history of an early Precambrian granulite-facies terrane, Jining District, South-East Inner-Mongolia, China. *J. Metamorph. Geol.* **1993**, *11*, 483–498.
34. Wan, Y.S.; Liu, D.Y.; Dong, C.Y.; Xu, Z.Y.; Wang, Z.J.; Wilde, S.A.; Yang, Y.H.; Liu, Z.H.; Zhou, H.Y. The Precambrian Khondalite Belt in the Daqingshan area, North China Craton: Evidence for multiple metamorphic events in the Palaeoproterozoic era. *Geol. Soc. Lond. Spec. Publ.* **2009**, *323*, 73–97. [CrossRef]
35. Dan, W.; Li, X.H.; Guo, J.H.; Liu, Y.; Wang, X.C. Integrated in situ zircon U–Pb age and Hf–O isotopes for the Helanshan khondalites in North China Craton: Juvenile crustal materials deposited in active or passive continental margin? *Precambrian Res.* **2012**, *222*, 143–158. [CrossRef]
36. Wang, L.J.; Guo, J.H.; Yin, C.Q.; Peng, P. Petrogenesis of ca. 1.95 Ga meta-leucogranites from the Jining Complex in the Khondalite Belt, North China Craton: Water-fluxed melting of metasedimentary rocks. *Precambrian Res.* **2017**, *303*, 355–371. [CrossRef]
37. Li, W.X.; Yin, C.Q.; Lin, S.F.; Li, W.J.; Gao, P.; Zhang, J.; Qian, J.H.; Qiao, H.Z. Paleoproterozoic tectonic evolution from subduction to collision of the Khondalite Belt in North China: Evidence from multiple magmatism in the Qianlishan Complex. *Precambrian Res.* **2022**, *368*, 106471. [CrossRef]
38. Yin, C.Q.; Zhao, G.C.; Xiao, W.J.; Lin, S.F.; Gao, R.; Zhang, J.; Qian, J.H.; Gao, P.; Qiao, H.Z.; Li, W.X. Paleoproterozoic accretion and assembly of the Western Block of North China: A new model. *Earth-Sci. Rev.* **2023**, *241*, 104448. [CrossRef]
39. Wan, Y.S.; Song, B.; Liu, D.Y.; Wilde, S.A.; Wu, J.S.; Shi, Y.R.; Yin, X.Y.; Zhou, H.Y. SHRIMP U–Pb zircon geochronology of Palaeoproterozoic metasedimentary rocks in the North China Craton: Evidence for a major Late Palaeoproterozoic tectonothermal event. *Precambrian Res.* **2006**, *149*, 249–271. [CrossRef]
40. Wan, Y.S.; Xu, Z.Y.; Dong, C.Y.; Nutman, A.; Ma, M.Z.; Xie, H.Q.; Liu, S.J.; Liu, D.Y.; Wang, H.C.; Cu, H. Episodic paleoproterozoic (~2.45, ~1.95 and ~1.85 Ga) mafic magmatism and associated high temperature metamorphism in the Daqingshan area, North China Craton: SHRIMP zircon U–Pb dating and whole-rock geochemistry. *Precambrian Res.* **2013**, *224*, 71–93. [CrossRef]
41. Xia, X.P.; Sun, M.; Zhao, G.C.; Luo, Y. LA-ICP-MS U–Pb geochronology of detrital zircons from the Jining Complex, North China Craton and its tectonic significance. *Precambrian Res.* **2006**, *144*, 199–212. [CrossRef]
42. Xia, X.P.; Sun, M.; Zhao, G.C.; Wu, F.Y.; Xu, P.; Zhang, J.H.; Luo, Y. U–Pb and Hf isotopic study of detrital zircons from the Wulashan khondalites: Constraints on the evolution of the Ordos Terrane, Western Block of the North China Craton. *Earth Planet. Sci. Lett.* **2006**, *241*, 581–593. [CrossRef]
43. Xia, X.P.; Sun, M.; Zhao, G.C.; Wu, F.Y.; Xu, P.; Zhang, J.; He, Y.H. Paleoproterozoic crustal growth in the Western Block of the North China Craton: Evidence from detrital zircon Hf and whole rock Sr-Nd isotopic compositions of the Khondalites from the Jining Complex. *Am. J. Sci.* **2008**, *308*, 304–327. [CrossRef]
44. Dong, C.Y.; Liu, D.Y.; Li, J.J.; Wan, Y.S.; Zhou, H.Y.; Li, C.D.; Yang, Y.H.; Xie, L.W. Palaeoproterozoic Khondalite Belt in the western North China Craton: New evidence from SHRIMP dating and Hf isotope composition of zircons from metamorphic rocks in the Bayan Ul-Helan Mountains area. *Chin. Sci. Bull.* **2007**, *52*, 2984–2994, (In Chinese with English Abstract). [CrossRef]
45. Dong, C.Y.; Wan, Y.S.; Xu, Z.Y.; Liu, D.Y.; Yang, Z.S.; Ma, M.Z.; Xie, H.Q. SHRIMP zircon U–Pb dating of late Paleoproterozoic kondalites in the Daqing Mountains area on the North China Craton. *Sci. China Earth Sci.* **2013**, *56*, 115–125. [CrossRef]
46. Yin, C.Q.; Zhao, G.C.; Guo, J.H.; Sun, M.; Xia, X.P.; Zhou, X.W.; Liu, C.H. U–Pb and Hf isotopic study of zircons of the Helanshan Complex: Constrains on the evolution of the Khondalite Belt in the Western Block of the North China Craton. *Lithos* **2011**, *122*, 25–38. [CrossRef]
47. Jiao, S.J.; Guo, J.H.; Harley, S.L.; Peng, P. Geochronology and trace element geochemistry of zircon, monazite and garnet from the garnetite and/or associated other high-grade rocks: Implications for Palaeoproterozoic tectonothermal evolution of the Khondalite Belt, North China Craton. *Precambrian Res.* **2013**, *237*, 78–100. [CrossRef]
48. Liu, P.H.; Liu, F.L.; Liu, C.H.; Liu, J.H.; Wang, F.; Xiao, L.L.; Cai, J.; Shi, J.R. Multiple mafic magmatic and high-grade metamorphic events revealed by zircons from meta-mafic rocks in the Daqingshan–Wulashan Complex of the Khondalite Belt, North China Craton. *Precambrian Res.* **2014**, *246*, 334–357. [CrossRef]
49. Liu, P.H.; Liu, F.L.; Cai, J.; Liu, C.H.; Liu, J.H.; Wang, F.; Xiao, L.L.; Shi, J.R. Spatial distribution, P–T–t paths, and tectonic significance of high-pressure mafic granulites from the Daqingshan–Wulashan Complex in the Khondalite Belt, North China Craton. *Precambrian Res.* **2017**, *303*, 687–708. [CrossRef]
50. Gou, L.L.; Zhang, C.L.; Brown, M.; Piccoli, P.M.; Lin, H.B.; Wei, X.S. P–T–t evolution of pelitic gneiss from the basement underlying the Northwestern Ordos Basin, North China Craton, and the tectonic implications. *Precambrian Res.* **2016**, *276*, 67–84. [CrossRef]
51. Cai, J.; Liu, F.L.; Liu, P.H. Paleoproterozoic multistage metamorphic events in Jining metapelitic rocks from the Khondalite Belt in the North China Craton: Evidence from petrology, phase equilibria modelling and U–Pb geochronology. *J. Asian Earth Sci.* **2017**, *138*, 515–534. [CrossRef]
52. Cai, J.; Liu, F.L.; Liu, P.H.; Wang, F.; Liu, C.H.; Shi, J.R. Anatectic record and P–T path evolution of metapelites from the Wulashan Complex, Khondalite Belt, North China Craton. *Precambrian Res.* **2017**, *303*, 10–29. [CrossRef]

53. Xu, X.F.; Gou, L.L.; Long, X.P.; Dong, Y.P.; Liu, X.M.; Zi, J.W.; Li, Z.H.; Zhang, C.L.; Liu, L.; Zhao, J. Phase equilibrium modelling and SHRIMP zircon U–Pb dating of medium-pressure pelitic granulites in the Helanshan complex of the Khondalite Belt, North China Craton, and their tectonic implications. *Precambrian Res.* **2018**, *314*, 62–75. [CrossRef]
54. Santosh, M.; Tsunogae, T.; Li, J.H.; Liu, S.J. Discovery of sapphirine-bearing Mg–Al granulites in the North China Craton: Implications for Paleoproterozoic ultrahigh temperature metamorphism. *Gondwana Res.* **2007**, *11*, 263–285. [CrossRef]
55. Jiao, S.J.; Fitzsimons, I.C.; Guo, J.H. Paleoproterozoic UHT metamorphism in the Daqingshan Terrane, North China Craton: New constraints from phase equilibria modeling and SIMS U–Pb zircon dating. *Precambrian Res.* **2017**, *303*, 208–227. [CrossRef]
56. Jiao, S.J.; Fitzsimons, I.C.; Zi, J.W.; Evans, N.J.; Mcdonald, B.J.; Guo, J.H. Texturally controlled U–Th–Pb monazite geochronology reveals Paleoproterozoic UHT metamorphic evolution in the Khondalite belt, North China craton. *J. Petrol.* **2020**, *61*, egaa023. [CrossRef]
57. Jiao, S.J.; Evans, N.J.; Guo, J.H.; Fitzsimons, I.C.W.; Zi, J.W.; McDonald, B.J. Establishing the PT path of UHT granulites by geochemically distinguishing peritectic from retrograde garnet. *Am. Mineral.* **2021**, *106*, 1640–1653. [CrossRef]
58. Gou, L.L.; Li, Z.H.; Liu, X.M.; Dong, Y.P.; Zhao, J.; Zhang, C.L.; Liu, L.; Long, X.P. Ultrahigh-temperature metamorphism in the Helanshan complex of the Khondalite Belt, North China Craton: Petrology and phase equilibria of spinel-bearing pelitic granulites. *J. Metamorph. Geol.* **2018**, *36*, 1199–1220. [CrossRef]
59. Gou, L.L.; Zi, J.W.; Dong, Y.P.; Liu, X.M.; Li, Z.H.; Xu, X.F.; Zhang, C.L.; Liu, L.; Long, X.P.; Zhao, Y.H. Timing of two separate granulite-facies metamorphic events in the Helanshan complex, North China Craton: Constraints from monazite and zircon U–Pb dating of pelitic granulites. *Lithos* **2019**, *350*, 105216. [CrossRef]
60. Jiao, S.J.; Guo, J.H. Paleoproterozoic UHT metamorphism with isobaric cooling (IBC) followed by decompression–heating in the Khondalite Belt (North China Craton): New evidence from two sapphirine formation processes. *J. Metamorph. Geol.* **2020**, *38*, 357–378. [CrossRef]
61. Zheng, Y.Y.; Qi, Y.; Zhang, D.; Jiao, S.J.; Huang, G.Y.; Guo, J.H. New insight from the first application of Ti-in-Quartz (TitaniQ) thermometry mapping in the eastern Khondalite Belt, North China Craton. *Front. Earth Sci.* **2022**, *10*, 860057. [CrossRef]
62. Wang, L.J.; Guo, J.H.; Yin, C.Q.; Peng, P.; Zhang, J.; Spencer, C.J.; Qian, J.H. High-temperature S-type granitoids (charnockites) in the Jining complex, North China Craton: Restite entrainment and hybridization with mafic magma. *Lithos* **2018**, *320–321*, 435–453. [CrossRef]
63. Wang, L.J.; Guo, J.H.; Peng, P. Petrogenesis of Paleoproterozoic Liangcheng garnet granitoids in the Khondalite Belt, North China Craton. *Acta Petrol. Sin.* **2021**, *37*, 375–390, (In Chinese with English Abstract).
64. Shi, Q.; Ding, D.; Xu, Z.Y.; Li, W.Q.; Li, G.; Li, C.X.; Zhao, Z.H.; Zhang, G.B.; Jiang, X.Y.; Yang, R.B.; et al. Metamorphic evolution of Daqingshan supracrustal rocks and garnet granite from the North China Craton: Constraints from phase equilibria modelling, geochemistry, and SHRIMP U–Pb geochronology. *Gondwana Res.* **2021**, *97*, 101–120. [CrossRef]
65. Jiang, X.Z.; Yu, S.Y.; Liu, Y.J.; Li, S.Z.; Lv, P.; Peng, Y.B.; Gao, X.Y.; Ji, W.T.; Li, C.Z.; Xie, W.M. Episodic metamorphism and anatexis within the Khondalite Belt, North China Craton: Constraint from Late-Paleoproterozoic fluid-fluxed melting of the Daqingshan Complex. *Precambrian Res.* **2022**, *369*, 106504. [CrossRef]
66. Qiao, H.Z. Detrital zircon U–Pb ages of the Huangqikou Formation of the Changcheng System in the Qianlishan Area, western North China Craton and their geological implications. *Acta Geol. Sichuan* **2021**, *41*, 33–39. (In Chinese with English Abstract)
67. Li, W.J. Geochronology and Geochemistry of the Helanshan-Qianlishan Granites in North China. Master's Dissertation, Sun Yat-sen University, Guangzhou, China, 2018; pp. 1–103, (In Chinese with English Abstract).
68. Lu, C.S.; Qian, J.H.; Yin, C.Q.; Gao, P.; Guo, M.J.; Zhang, W.F. Ultrahigh temperature metamorphism recorded in the Lüliang Complex, Trans-North China Orogen: P–T–t evolution and heating mechanism. *Precambrian Res.* **2022**, *383*, 106900. [CrossRef]
69. Wiedenbeck, M.; Allé, P.; Corfu, F.; Griffin, W.L.; Meier, M.; Oberli, F.; Quadt, A.; Roddick, J.C.; Spiegel, W. Three natural zircon standards for U-Th-Pb, Lu-Hf, trace element and REE analyses. *Geostand. Newsl.* **1995**, *19*, 1–23. [CrossRef]
70. Reed, W. *Certificate of Analysis: Standard Reference Materials 610 and 611*; National Institute of Standards and Technology: Gaithersburg, MD, USA, 1992.
71. Sláma, J.; Kosler, J.; Condon, D.; Crowley, J.L.; Gerdes, A.; Hanchar, J.M.; Horstwood, M.S.A.; Morris, G.A.; Nasdala, L.; Norberg, N.; et al. Plešovice zircon–A new natural reference material for U–Pb and Hf isotopic microanalysis. *Chem. Geol.* **2008**, *249*, 1–35. [CrossRef]
72. Liu, Y.S.; Hu, Z.C.; Gao, S.; Günther, D.; Xu, J.; Gao, C.G.; Chen, H.H. In situ analysis of major and trace elements of anhydrous minerals by LA-ICP-MS without applying an internal standard. *Chem. Geol.* **2008**, *257*, 34–43. [CrossRef]
73. Ludwig, K.R. *Isoplot/Ex Version 4.15: A Geochronological Toolkit for Microsoft Excel*; Berkeley Geochronology Center Special Publication: Berkeley, CA, USA, 2012; Volume 5, p. 75.
74. Rubatto, D. Zircon trace element geochemistry: Partitioning with garnet and the link between U–Pb ages and metamorphism. *Chem. Geol.* **2002**, *184*, 123–138. [CrossRef]
75. Ramsay, J.G. *Folding and Fracturing of Rocks*; McGraw-Hill: New York, NY, USA, 1967; p. 568.
76. Liu, S.J.; Dong, C.Y.; Xu, Z.Y.; Santosh, M.; Ma, M.Z.; Xie, H.Q.; Liu, D.Y.; Wan, Y.S. Palaeoproterozoic episodic magmatism and high-grade metamorphism in the North China Craton: Evidence from SHRIMP zircon dating of magmatic suites in the Daqingshan area. *Geol. J.* **2013**, *48*, 429–455. [CrossRef]

77. Li, W.J.; Yin, C.Q.; Long, X.P.; Zhang, J.; Xia, X.P.; Wang, L.J. Paleoproterozoic S-type granites from the Helanshan Complex in Inner Mongolia: Constraints on the provenance and the Paleoproterozoic evolution of the Khondalite Belt, North China Craton. *Precambrian Res.* **2017**, *299*, 195–209. [CrossRef]
78. Qiao, H.Z.; Yin, C.Q.; Xiao, W.J.; Zhang, J.; Qian, J.H.; Wu, S.J. Paleoproterozoic polyphase deformation in the Helanshan Complex: Structural and geochronological constraints on the tectonic evolution of the Khondalite Belt, North China Craton. *Precambrian Res.* **2022**, *368*, 106468. [CrossRef]
79. Gan, S.F.; Qian, X.L. A plate-tectonic model for the evolution of the Daqingshan granulite belt in Inner Mongolia, China. *Acta Geol. Sin.* **1996**, *70*, 298–308, (In Chinese with English Abstract).
80. Yu, H.F.; Sun, D.Y. Deformational-Metamorphic Evolution of Ductile Shear Zone in Daqingshan Area. *J. Chang. Univ. Earth Sci.* **1996**, *26*, 310–315, (In Chinese with English Abstract).
81. Liu, T.J.; Li, W.M.; Liu, Y.J.; Jin, W.; Shao, Y.L. Rheology of the anatectic mid-lower Crust in the Paleoproterozoic orogenic belt in Daqingshan. Inner Mongolia. *Acta Petrol. Sin.* **2020**, *55*, 459–486, (In Chinese with English Abstract).
82. Liu, T.J.; Li, W.M.; Liu, Y.J.; Jin, W.; Zhao, Y.L.; Iqbal, M.Z. Deformation characteristics of the high-grade metamorphic and anatectic rocks in the Daqingshan Paleoproterozoic orogenic belt, Inner Mongolia: A case study from the Shijiaqu-Xuehaigou area. *Precambrian Res.* **2022**, *374*, 106644. [CrossRef]
83. Xu, Z.Y.; Liu, Z.H.; Yang, Z.S. Structures of early metamorphic strata in the khondalite series in the Daqingshan-Wulashan area, Inner Mongolia: Results of the sub-horizontal bedding-parallel detachment deformation in the lower crust. *J. Stratigr.* **2005**, *29*, 423–432, (In Chinese with English Abstract).
84. Xu, Z.Y.; Liu, Z.H.; Yang, Z.S.; Wu, X.W.; Chen, X.F. Structure of metamorphic strata of the khondalite series in the Daqingshan-Wulashan area, central Inner Mongolia, China, and their geodynamic implications. *Geol. Bull. China* **2007**, *26*, 526–536. (In Chinese with English Abstract)
85. Liu, Z.H.; Pan, B.W.; Li, P.C.; Zhu, K.; Dong, X. Ductile Shear Zone in High-Grade Metamorphic Rocks and Its Rheomorphic Mechanism in the Daqing Mountain Area, Inner Mongolia. *Earth Sci.* **2017**, *42*, 2105–2116, (In Chinese with English Abstract).
86. Qiao, H.Z.; Yin, C.Q.; Zhang, J.; Qian, J.H.; Wu, S.J. New Discovery of ~1866 Ma high-temperature mylonite in the Helanshan Complex: Marking a late-stage ductile shearing in the Khondalite Belt, North China Craton. *Acta Geol. Sin. (Engl. Ed.)* **2021**, *95*, 1418–1419. [CrossRef]